

Constraints on Large Extra Dimensions from the MINOS Experiment

P. Adamson,⁸ I. Anghel,^{15,1} A. Aurisano,⁷ G. Barr,²² M. Bishai,³ A. Blake,^{5,16} G. J. Bock,⁸ D. Bogert,⁸ S. V. Cao,³⁰ T. J. Carroll,³⁰ C. M. Castromonte,⁹ R. Chen,¹⁸ S. Childress,⁸ J. A. B. Coelho,³¹ L. Corwin,^{14,*} D. Cronin-Hennessy,¹⁹ J. K. de Jong,²² S. De Rijck,³⁰ A. V. Devan,³³ N. E. Devenish,²⁸ M. V. Diwan,³ C. O. Escobar,⁶ J. J. Evans,¹⁸ E. Falk,²⁸ G. J. Feldman,¹⁰ W. Flanagan,³⁰ M. V. Frohne,^{11,†} M. Gabrielyan,¹⁹ H. R. Gallagher,³¹ S. Germani,¹⁷ R. A. Gomes,⁹ M. C. Goodman,¹ P. Gouffon,²⁵ N. Graf,²³ R. Gran,²⁰ K. Grzelak,³² A. Habig,²⁰ S. R. Hahn,⁸ J. Hartnell,²⁸ R. Hatcher,⁸ A. Holin,¹⁷ J. Huang,³⁰ J. Hylen,⁸ G. M. Irwin,²⁷ Z. Isvan,³ C. James,⁸ D. Jensen,⁸ T. Kafka,³¹ S. M. S. Kasahara,¹⁹ G. Koizumi,⁸ M. Kordosky,³³ A. Kreymer,⁸ K. Lang,³⁰ J. Ling,³ P. J. Litchfield,^{19,24} P. Lucas,⁸ W. A. Mann,³¹ M. L. Marshak,¹⁹ N. Mayer,³¹ C. McGivern,²³ M. M. Medeiros,⁹ R. Mehdiev,³⁰ J. R. Meier,¹⁹ M. D. Messier,¹⁴ W. H. Miller,¹⁹ S. R. Mishra,²⁶ S. Moed Sher,⁸ C. D. Moore,⁸ L. Mualem,⁴ J. Musser,¹⁴ D. Naples,²³ J. K. Nelson,³³ H. B. Newman,⁴ R. J. Nichol,¹⁷ J. A. Nowak,^{19,‡} J. O'Connor,¹⁷ M. Orchanian,⁴ R. B. Pahlka,⁸ J. Paley,¹ R. B. Patterson,⁴ G. Pawloski,¹⁹ A. Perch,¹⁷ M. M. Pfützner,¹⁷ D. D. Phan,³⁰ S. Phan-Budd,¹ R. K. Plunkett,⁸ N. Poonthottathil,⁸ X. Qiu,²⁷ A. Radovic,³³ B. Rebel,⁸ C. Rosenfeld,²⁶ H. A. Rubin,¹³ P. Sail,³⁰ M. C. Sanchez,^{15,1} J. Schneps,³¹ A. Schreckenberger,³⁰ P. Schreiner,¹ R. Sharma,⁸ A. Sousa,⁷ N. Tagg,²¹ R. L. Talaga,¹ J. Thomas,¹⁷ M. A. Thomson,⁵ X. Tian,²⁶ A. Timmons,¹⁸ J. Todd,⁷ S. C. Tognini,⁹ R. Toner,¹⁰ D. Torretta,⁸ G. Tzanakos,^{2,†} J. Urheim,¹⁴ P. Vahle,³³ B. Viren,³ A. Weber,^{22,24} R. C. Webb,²⁹ C. White,¹³ L. Whitehead,¹² L. H. Whitehead,¹⁷ S. G. Wojcicki,²⁷ and R. Zwaska⁸

(The MINOS Collaboration)

¹Argonne National Laboratory, Argonne, Illinois 60439, USA

²Department of Physics, University of Athens, GR-15771 Athens, Greece

³Brookhaven National Laboratory, Upton, New York 11973, USA

⁴Lauritsen Laboratory, California Institute of Technology, Pasadena, California 91125, USA

⁵Cavendish Laboratory, University of Cambridge, Cambridge CB3 0HE, United Kingdom

⁶Universidade Estadual de Campinas, IFGW, CP 6165, 13083-970, Campinas, SP, Brazil

⁷Department of Physics, University of Cincinnati, Cincinnati, Ohio 45221, USA

⁸Fermi National Accelerator Laboratory, Batavia, Illinois 60510, USA

⁹Instituto de Física, Universidade Federal de Goiás, 74690-900, Goiânia, GO, Brazil

¹⁰Department of Physics, Harvard University, Cambridge, Massachusetts 02138, USA

¹¹Holy Cross College, Notre Dame, Indiana 46556, USA

¹²Department of Physics, University of Houston, Houston, Texas 77204, USA

¹³Department of Physics, Illinois Institute of Technology, Chicago, Illinois 60616, USA

¹⁴Indiana University, Bloomington, Indiana 47405, USA

¹⁵Department of Physics and Astronomy, Iowa State University, Ames, Iowa 50011 USA

¹⁶Lancaster University, Lancaster, LA1 4YB, UK

¹⁷Department of Physics and Astronomy, University College London, London WC1E 6BT, United Kingdom

¹⁸School of Physics and Astronomy, University of Manchester, Manchester M13 9PL, United Kingdom

¹⁹University of Minnesota, Minneapolis, Minnesota 55455, USA

²⁰Department of Physics, University of Minnesota Duluth, Duluth, Minnesota 55812, USA

²¹Otterbein University, Westerville, Ohio 43081, USA

²²Subdepartment of Particle Physics, University of Oxford, Oxford OX1 3RH, United Kingdom

²³Department of Physics and Astronomy, University of Pittsburgh, Pittsburgh, Pennsylvania 15260, USA

²⁴Rutherford Appleton Laboratory, Science and Technology Facilities Council, Didcot, OX11 0QX, United Kingdom

²⁵Instituto de Física, Universidade de São Paulo, CP 66318, 05315-970, São Paulo, SP, Brazil

²⁶Department of Physics and Astronomy, University of South Carolina, Columbia, South Carolina 29208, USA

²⁷Department of Physics, Stanford University, Stanford, California 94305, USA

²⁸Department of Physics and Astronomy, University of Sussex, Falmer, Brighton BN1 9QH, United Kingdom

²⁹Physics Department, Texas A&M University, College Station, Texas 77843, USA

³⁰Department of Physics, University of Texas at Austin, Austin, Texas 78712, USA

³¹Physics Department, Tufts University, Medford, Massachusetts 02155, USA

³²Department of Physics, University of Warsaw, PL-02-093 Warsaw, Poland

³³Department of Physics, College of William & Mary, Williamsburg, Virginia 23187, USA

(Dated: January 25, 2017)

We report new constraints on the size of large extra dimensions from data collected by the MINOS experiment between 2005 and 2012. Our analysis employs a model in which sterile neutrinos arise as Kaluza-Klein states in large extra dimensions and thus modify the neutrino oscillation probabilities due to mixing between active and sterile neutrino states. Using Fermilab's NuMI beam exposure

of 10.56×10^{20} protons-on-target, we combine muon neutrino charged current and neutral current data sets from the Near and Far Detectors and observe no evidence for deviations from standard three-flavor neutrino oscillations. The ratios of reconstructed energy spectra in the two detectors constrain the size of large extra dimensions to be smaller than $0.45 \mu\text{m}$ at 90% C.L. in the limit of a vanishing lightest active neutrino mass. Stronger limits are obtained for non-vanishing masses.

PACS numbers: 14.60.St, 14.60.Pq, 04.50.+h

Neutrino oscillation has been established through measurements of solar, atmospheric, reactor, and accelerator beam neutrinos [1–7]. The underlying mechanism can be described by the unitary PMNS mixing matrix [8], which connects the three weak flavor eigenstates (ν_e, ν_μ, ν_τ) with the three mass eigenstates (ν_1, ν_2, ν_3). This matrix can be parameterized by three mixing angles, θ_{12} , θ_{13} , and θ_{23} , and a CP-violating phase δ_{CP} . Oscillation probabilities in vacuum depend upon the mixing parameters, neutrino energy, travel distance (baseline), and the squared neutrino mass differences $\Delta m_{ij}^2 \equiv m_i^2 - m_j^2$ ($i, j = 1, 2, 3$). Oscillation probabilities in long-baseline experiments can be further modified by matter effects [9].

Current data are well described by the three-flavor model. However, with increasing precision of experiments, one can test for discrepancies that could be accounted for by small modifications to the standard three-flavor model. One such scenario employs large extra dimensions.

Sub-millimeter sized large extra dimensions were originally introduced in [10] to explain the large gap between the electroweak scale, $m_{\text{EW}} \sim 10^3 \text{ GeV}$, and the Planck scale, $M_{\text{Pl}} \sim 10^{19} \text{ GeV}$. In this model, M_{Pl} attains its high value due to a volumetric scaling of a more fundamental scale, \overline{M}_{Pl} , which is assumed to be of the same order of magnitude as m_{EW} ,

$$M_{\text{Pl}}^2 = \overline{M}_{\text{Pl}}^{d+2} V_d, \quad (1)$$

where d is the number of extra dimensions and V_d the corresponding volume. In this framework, however, the lack of a higher fundamental scale disqualifies the see-saw mechanism [11] as an explanation of the small neutrino masses. To resolve this, the existence of sterile neutrinos, arising as Kaluza-Klein (KK) states in the extra dimensions, is suggested in [12, 13], leading to small Dirac neutrino masses [13]

$$m_\nu = \kappa v \frac{\overline{M}_{\text{Pl}}}{M_{\text{Pl}}}, \quad (2)$$

where κ is a Yukawa coupling coefficient and v the Higgs vacuum expectation value.

Adopting the Large Extra Dimension (LED) model of [14–18], all the Standard Model (SM) fields, including the three left-handed (active) neutrinos and the Higgs doublet, live on a four-dimensional brane, 3+1 spacetime. Three SM singlet fermion fields, one for each neutrino flavor, live in a higher-dimensional bulk, 3+1+ d spacetime,

with at least two compactified extra dimensions ($d \geq 2$). To simplify matters, one of the extra dimensions can be compactified on a circle with radius R much larger than the size of the other dimensions, effectively making this a five-dimensional problem. The compactness of the extra dimension allows a decomposition of each bulk fermion in Fourier modes. From the couplings to gauge bosons, the zero modes can be identified as the active neutrinos, while the other modes are sterile neutrinos. All these states are collectively referred to as the KK towers. The Yukawa coupling between the bulk fermions and the active neutrinos leads to mixing between the SM and KK neutrinos, which alters the three-flavor oscillation probabilities. Hence, neutrino oscillation measurements can constrain the size of large extra dimensions.

As discussed in [18], the oscillation amplitude among active neutrino states can be written as

$$\mathcal{A}(\nu_\alpha \rightarrow \nu_\beta) = \sum_{i,j,k=1}^3 \sum_{n=0}^{+\infty} U_{\alpha i} U_{\beta k}^* W_{ij}^{(0n)*} W_{kj}^{(0n)} \times \exp \left[i \left(\frac{\lambda_j^{(n)}}{R} \right)^2 \left(\frac{L}{2E} \right) \right], \quad (3)$$

where E is the neutrino energy and L the baseline. The eigenvalues $\lambda_j^{(n)}$ of the Hamiltonian depend on R and the active neutrino masses m_1 , m_2 , and m_3 . The matrices U and W are the mixing matrices for the active and KK neutrino modes, respectively. The $(0n)$ indices refer to the mixing between the zero mode and the KK tower. In practice, only the first five KK modes are considered in each tower [18]. Squaring the amplitude gives the oscillation probability $P(\nu_\alpha \rightarrow \nu_\beta)$. Compared to the three-flavor case, this model requires two extra parameters, R and m_0 , where the latter is defined as the lightest active neutrino mass (normal mass ordering: $m_3 > m_2 > m_1 \equiv m_0$; inverted mass ordering: $m_2 > m_1 > m_3 \equiv m_0$).

In Fig. 1, the muon neutrino survival probability, $P(\nu_\mu \rightarrow \nu_\mu)$, for the MINOS baseline and normal mass ordering, is illustrated for $m_0 = 0 \text{ eV}$ and two values of R . As stated in [18], there are three prominent features of LED visible in this figure: a displacement of the oscillation minimum with respect to the three-flavor case, a reduction of the integrated survival probability because of active-to-KK oscillation, and the appearance of modulations on the survival probability because of fast oscillations to the KK states. With increasing energy, the

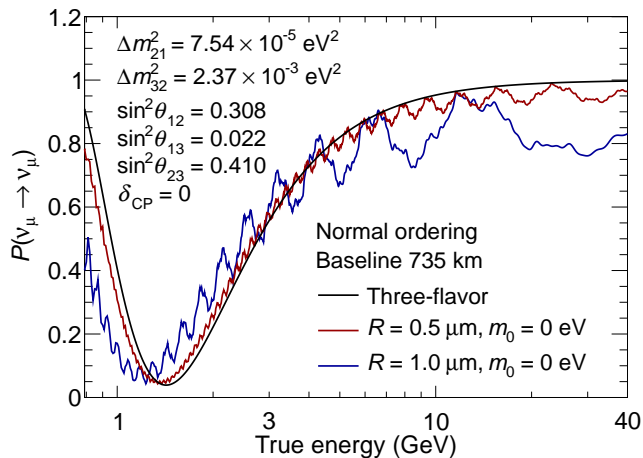


FIG. 1: The muon neutrino survival probability $P(\nu_\mu \rightarrow \nu_\mu)$ at the MINOS Far Detector as a function of the true neutrino energy for $m_0 = 0$ eV and $R = 0.5 \mu\text{m}$ (red line) or $1 \mu\text{m}$ (blue line), and for three-flavor oscillation (black line).

amplitude of the modulations increases while their frequency decreases, making the effects of LED easier to observe away from the oscillation minimum. The values in Fig. 1 of $\Delta m_{32}^2 = 2.37 \times 10^{-3} \text{eV}^2$ and $\sin^2 \theta_{32} = 0.410$ are taken from the MINOS standard oscillation analysis [3]. The value of $\sin^2 \theta_{13} = 0.022$ is a weighted average of the Daya Bay [19], RENO [20], and Double Chooz [21] results. The values of $\Delta m_{21}^2 = 7.54 \times 10^{-5} \text{eV}^2$ and $\sin^2 \theta_{12} = 0.308$ are taken from a global fit [22]. We set $\delta_{\text{CP}} = 0$ since it has little effect on the oscillation probabilities [23]. These values are used throughout the analysis.

Constraints on this model based on atmospheric, reactor, and accelerator beam neutrino oscillation experiments are discussed in [17]. The authors derived a bound constraining R to be less than $0.82 \mu\text{m}$ at 90% C.L. The sensitivities of CHOOZ, KamLAND, and MINOS for this model were calculated in [18] using a modified version of the GLoBES software [24]. Assuming 7.24×10^{20} protons-on-target (POT) for MINOS in ν_μ mode, a combined sensitivity of $R < 0.75$ ($0.49 \mu\text{m}$) at 90% C.L. was obtained for normal (inverted) mass ordering and vanishing m_0 . The zenith distribution of atmospheric neutrino events collected by IceCube was analyzed in [25], where the authors showed that it is possible to exclude $R \gtrsim 0.40 \mu\text{m}$ at 95% C.L. The above neutrino limits are about two orders of magnitude stronger than those obtained from tabletop gravitational experiments [26]. Astrophysical and cosmological bounds are often much more stringent, but are model-dependent [26]. Collider experiments can set limits on the volume of the extra dimensions [26]. This paper presents an analysis, sensitive to LED, of the MINOS data set with a low-energy ν_μ mode exposure of 10.56×10^{20} POT and a peak neutrino energy of 3 GeV.

In the MINOS experiment, neutrinos are produced by

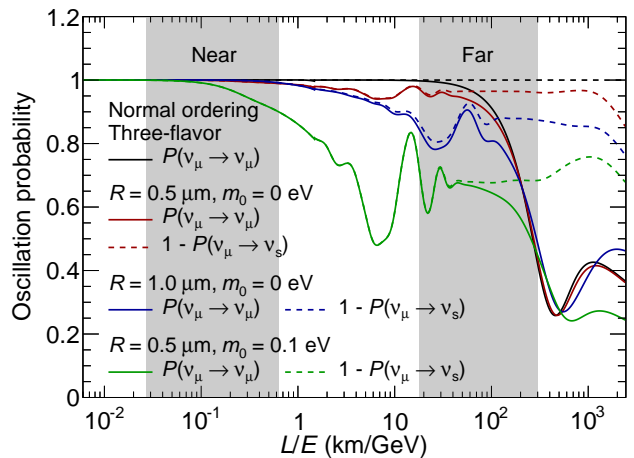


FIG. 2: The oscillation probabilities as a function of L/E , incorporating MINOS energy resolution effects, for the three-flavor case (black line), the same LED scenarios as in Fig. 1 (red and blue lines), and an LED case with non-zero m_0 (green lines). The baseline and neutrino energy are denoted as L and E , respectively. The L/E coverage of the Near Detector and Far Detector are represented by the grey bands, which contain 90% of the MINOS data.

directing 120 GeV protons from the Fermilab Main Injector onto a graphite target. The resulting π and K mesons are focused in the forward direction and charge-sign selected by two magnetic horns after which they decay into neutrinos in a 675 m long tunnel. MINOS observes charged current (CC) and neutral current (NC) neutrino events in a Near Detector (ND) and Far Detector (FD) located 1.04 km and 735 km downstream of the target, respectively, on the NuMI (Neutrinos at the Main Injector) beamline axis [27]. The beam composition at the ND consists of 91.8% ν_μ , 6.9% $\bar{\nu}_\mu$, and 1.3% ν_e and $\bar{\nu}_e$ when operating in ν_μ mode. The ND and FD are tracking-sampling calorimeters built of 2.54 cm thick iron plates interleaved with scintillator planes composed of 1 cm thick, 4.1 cm wide strips, arranged in two alternating orthogonal views, and read out using wavelength-shifting fibers coupled to multi-anode photomultiplier tubes. The ND has a 23.7 t fiducial (980 t total) mass. The FD has a 4.2 kt fiducial (5.4 kt total) mass. Using magnetic coils, both detectors are magnetized with a toroidal magnetic field oriented to focus negatively charged particles when operating in ν_μ mode [28].

A ν_μ CC-like event ($\nu_\mu N \rightarrow \mu X$) in the MINOS detectors is characterized by a single outgoing muon track with possible hadronic showers near the event vertex. The muon momentum is determined from the track range for tracks confined within the detector and from the track curvature for exiting tracks. Since no charge separation is applied in this analysis, both ν_μ and $\bar{\nu}_\mu$ events are used. The energy of CC hadronic showers is estimated using a k -nearest-neighbor (k NN) algorithm based on the

shower topology, in addition to the calorimetric shower energy [29–33]. The CC neutrino energy at the FD is reconstructed with a mean resolution of 17.3% by summing the track and shower energies.

A ν_α NC-like event ($\nu_\alpha N \rightarrow \nu_\alpha X$ with $\alpha = e, \mu, \tau$) in the ND or FD has a short diffuse hadronic shower and possibly short hadron tracks. The NC event length is required to be shorter than 47 planes. If a hadron track is reconstructed in an event, the track length is required not to exceed the shower length by more than five planes. Additional selection requirements are imposed in the ND to remove cases where reconstruction failed due to high event rates [34, 35]. The NC neutrino energy at the FD is reconstructed with a mean resolution of 41.7% using the calorimetric shower energy.

In the CC selection procedure, separation between CC and NC events is performed by combining four variables describing track properties into a single discriminant variable using a k NN algorithm [36, 37]. Only events that failed the NC selection procedure are considered in the CC selection procedure. The selected CC sample has an efficiency (purity) estimated by Monte Carlo (MC) of 53.9% (98.7%) at the ND and 84.6% (99.1%) at the FD. The ND efficiency is low because events occurring near the magnetic coil hole are rejected. NC events are the main background in both detectors [23].

The selected NC sample has an efficiency (purity) estimated by MC of 79.9% (58.9%) at the ND and 87.6% (61.3%) at the FD. The background composition is 86.9% CC ν_μ and 13.1% beam CC ν_e at the ND. Assuming three-flavor oscillation, the backgrounds at the FD are estimated as 73.8% CC ν_μ , 21.6% CC ν_e , and 4.6% CC ν_τ [23].

The muon neutrino survival probability $P(\nu_\mu \rightarrow \nu_\mu)$, probed by CC events, and the sterile neutrino appearance probability $P(\nu_\mu \rightarrow \nu_s)$, probed by a depletion of NC events, are shown as a function of L/E in Fig. 2. The same two LED scenarios as in Fig. 1 and a scenario with non-zero m_0 are compared to the three-flavor case. MINOS energy resolution effects [38, 39] were accounted for when calculating the probabilities.

In the MINOS standard oscillation analysis [3], ND data are used to constrain the FD prediction based on the assumption of no oscillations along the ND baseline (black line in Fig. 2). In the LED analysis, this assumption is not valid for $m_0 \gtrsim 30$ meV when $R \gtrsim 0.01 \mu\text{m}$ (as illustrated by the green lines in Fig. 2), and a fit is performed to the ratio of the reconstructed FD and ND neutrino energy spectra. This Far-over-Near ratio fit, using a covariance-matrix-based χ^2 method [23], allows the analysis to be sensitive to oscillations along the ND and FD baselines and significantly reduces many systematics affecting both detectors. Figure 3 compares the Far-over-Near ratio of the MINOS CC and NC data to the three-flavor predictions and the LED predictions of the χ^2 minimum. The good agreement between data and the

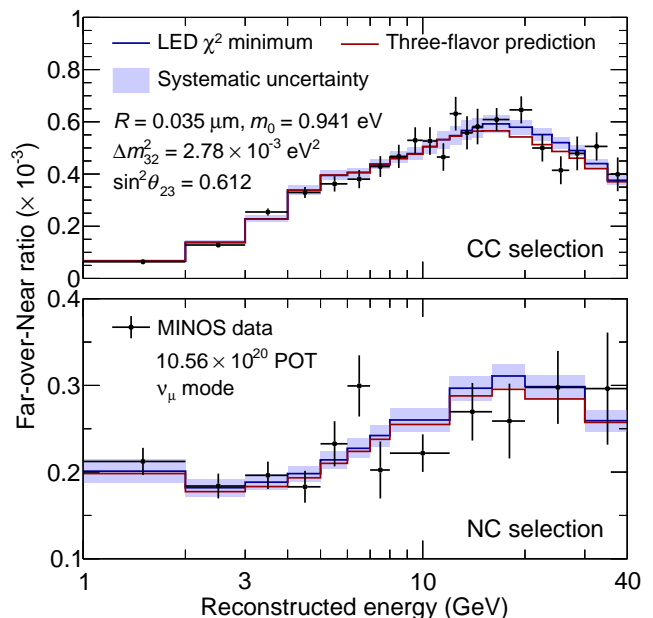


FIG. 3: The Far-over-Near ratio of the MINOS CC (top) and NC (bottom) data (black points) as a function of the reconstructed neutrino energy. The error bars represent statistical uncertainties. The three-flavor predictions, using the same oscillation parameters as Fig. 1, are shown in red. The LED predictions of the χ^2 minimum are shown with their systematic uncertainty (blue line and band).

three-flavor predictions indicates that, if large extra dimensions exist, oscillation between active and KK states must be sub-dominant in MINOS.

The energy window for the fit is set between 0 and 40 GeV, with the CC and NC binning schemes chosen such that the minimum number of FD events in a bin provides a good Gaussian approximation. The CC and NC samples are fitted simultaneously to improve the sensitivity. The total χ^2 is the sum of those of the CC and NC samples, with each one given by

$$\chi^2 = \sum_{i,j=1}^N (o_i - p_i)[V^{-1}]_{ij}(o_j - p_j) + \left(\frac{N_{\text{data}} - N_{\text{MC}}}{\sigma_N} \right)^2, \quad (4)$$

where o_i and p_i are the observed and predicted Far-over-Near ratios in energy bin i , respectively, and V is the sum of statistical and systematic covariance matrices. The second term is an ND beam flux penalty term, where N_{data} (N_{MC}) is the total number of ND data (MC) events, and $\sigma_N = 50\% N_{\text{MC}}$ is adopted as a conservative difference between hadron production measurements and MC calculations [23].

The total covariance matrix is

$$V = V_{\text{stat}} + V_{\text{acc}} + V_{\text{norm}} + V_{\text{NC}} + V_{\text{other}}. \quad (5)$$

The statistical uncertainties are contained in V_{stat} and

are less than 24% in each energy bin and 15% on average. The acceptance (V_{acc}), normalization (V_{norm}), and NC selection (V_{NC}) covariance matrices have the biggest impact on the sensitivity and are discussed below. Other systematic uncertainties (V_{other}), including neutrino interaction cross-section uncertainties and NuMI beam flux uncertainties, are small and have a cumulative effect of less than 4% in any energy bin of the Far-over-Near ratio.

The uncertainty in the acceptance and efficiency of the ND for CC and NC events is evaluated by varying event selection requirements in data and MC. Any shift in the data-MC agreement is taken as a systematic uncertainty. The effect on the Far-over-Near ratio of this systematic uncertainty is energy-dependent, never exceeding 6% (0.6%) for the CC (NC) sample, and includes correlations between different bins.

The normalization systematic uncertainty is a consequence of the detector differences between ND and FD, including material dimensions, detector live time, and reconstruction efficiencies. It has a uniform uncertainty in the Far-over-Near ratio of 1.6% (2.2%) for the CC (NC) sample.

The matrix V_{NC} accounts for the uncertainty in the selection procedure that reduces the number of poorly-reconstructed NC events, defined as those events with reconstructed energy less than 30% of the true energy. To improve data-MC agreement, the fraction of poorly reconstructed events in the simulation is varied in a template fit to the selection variables. The selection criteria are then adjusted to yield the same number of rejected events in data and MC. The variations seen in the NC energy spectra from this procedure are taken as a systematic uncertainty. In the Far-over-Near ratio, this uncertainty varies from 5% at 1 GeV to 1% at 10 GeV.

In minimizing the χ^2 in the (R, m_0) plane, θ_{23} and Δm_{32}^2 are free to vary in the fit. The four-dimensional parameter space is divided into $51 \times 51 \times 26 \times 51$ bins and has ranges $[10^{-8}, 10^{-6}]$ m, $[10^{-3}, 1]$ eV, $[0, \pi/2]$, and $[0, 5 \times 10^{-3}]$ eV² for R , m_0 , θ_{23} , and Δm_{32}^2 , respectively. The Far-over-Near ratio is calculated at each bin center and multilinear interpolation is used to obtain the Far-over-Near ratio at other points in the parameter space. Two initial θ_{23} hypotheses, one in each octant, are used in the fit. Since the mass ordering was shown to have little effect on the MINOS sensitivity [18, 23], only normal ordering is considered in this analysis. The parameters Δm_{21}^2 , θ_{12} , θ_{13} , and δ_{CP} are fixed to the values shown in Fig. 1. CPT symmetry is assumed, implying identical ν and $\bar{\nu}$ oscillation parameters [42, 43]. The 90% C.L. sensitivity contour and the cumulative effect of the systematic uncertainties are shown in Fig. 4. The sensitivity is calculated using simulated three-flavor data generated for the oscillation parameter values shown in Fig. 1.

The Feldman-Cousins technique [44] is used to obtain the 90% C.L. data contour shown in Fig. 5. A shallow global minimum is found at $R = 0.035 \mu\text{m}$, $m_0 =$

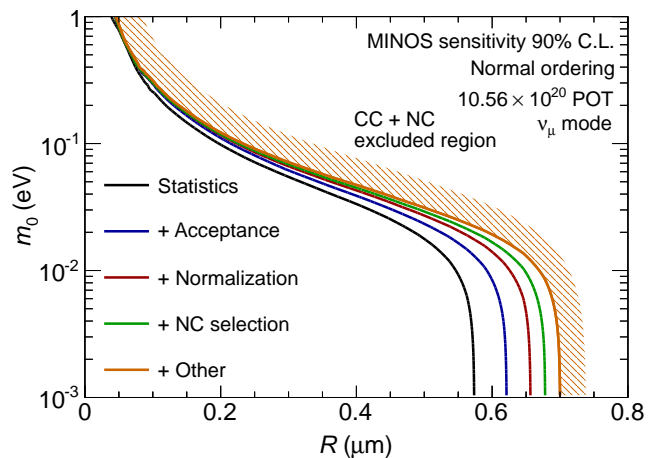


FIG. 4: The cumulative effect of the systematic uncertainties on the 90% C.L. sensitivity contour based on 10.56×10^{20} POT MC and assuming normal mass ordering. The large extra dimension size and the smallest neutrino mass are denoted as R and m_0 , respectively. The shaded area indicates the excluded region to the right of the contour.

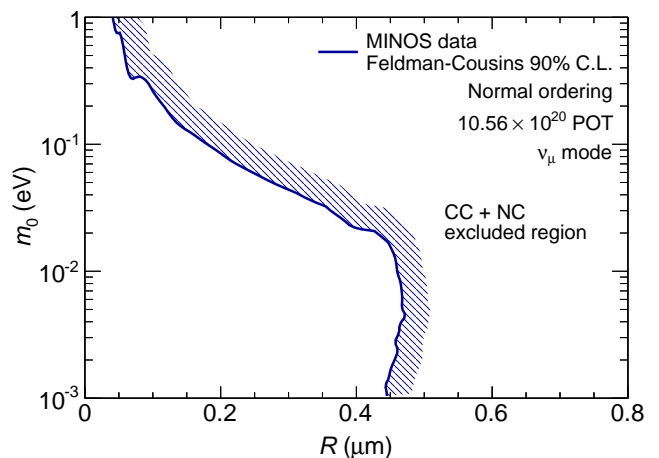


FIG. 5: The 90% C.L. data contour for the LED model, obtained using the Feldman-Cousins technique, based on 10.56×10^{20} POT MINOS data and assuming normal mass ordering. The large extra dimension size and the smallest neutrino mass are denoted as R and m_0 , respectively. The shaded area indicates the excluded region to the right of the contour.

0.941 eV, $\sin^2 \theta_{23} = 0.612$, and $\Delta m_{32}^2 = 2.78 \times 10^{-3}$ eV² with $\chi_{3\text{-flavor}}^2 - \chi_{\text{LED}}^2 = 0.95$. No evidence for large extra dimensions is found. The limit obtained from the data is stronger than expected from the sensitivity, as can be seen from a comparison of Figs. 4 and 5. A study of 1000 simulated experiments, each one using a Gaussian fluctuation of the simulated three-flavor data based on the full covariance matrices, shows that 39% of simulated experiments obtain an exclusion stronger than that obtained from the data at $m_0 = 0.005$ eV. In the limit of a vanishing lightest neutrino mass, the large extra dimension size

is constrained to be smaller than $0.45 \mu\text{m}$ at 90% C.L. To date, this is the strongest limit on this large extra dimension model [17, 18] reported by a neutrino oscillation experiment.

This work was supported by the U.S. DOE; the United Kingdom STFC; the U.S. NSF; the State and University of Minnesota; and Brazil's FAPESP, CNPq and CAPES. We are grateful to the Minnesota Department of Natural Resources and the personnel of the Soudan Laboratory and Fermilab. We thank the Texas Advanced Computing Center at The University of Texas at Austin for the provision of computing resources. We wish to thank P. A. N. Machado for providing insightful comments on the LED model.

* Now at South Dakota School of Mines and Technology, Rapid City, South Dakota 57701, USA.

† Deceased.

‡ Now at Lancaster University, Lancaster, LA1 4YB, UK.

- [1] Y. Ashie *et al.* (Super-Kamiokande Collaboration), Phys. Rev. Lett. **93**, 101801 (2004); Phys. Rev. D **71**, 112005 (2005).
- [2] B. Aharmim *et al.* (SNO Collaboration), Phys. Rev. C **72**, 055502 (2005).
- [3] D. G. Michael *et al.* (MINOS Collaboration), Phys. Rev. Lett. **97**, 191801 (2006); P. Adamson *et al.* (MINOS Collaboration), Phys. Rev. D **77**, 072002 (2008); Phys. Rev. Lett. **112**, 191801 (2014).
- [4] T. Araki *et al.* (KamLAND Collaboration), Phys. Rev. Lett. **94**, 081801 (2005).
- [5] C. Arpesella *et al.* (Borexino Collaboration), Phys. Rev. Lett. **101**, 091302 (2008).
- [6] M. H. Ahn *et al.* (K2K Collaboration), Phys. Rev. D **74**, 072003 (2006).
- [7] F. P. An *et al.* (Daya Bay Collaboration), Phys. Rev. Lett. **108**, 171803 (2012); J. K. Ahn *et al.* (RENO Collaboration), Phys. Rev. Lett. **108**, 191802 (2012).
- [8] B. Pontecorvo, Sov. Phys. JETP **7**, 172 (1958); Z. Maki, M. Nakagawa, and S. Sakata, Prog. Theor. Phys. **28**, 870 (1962); V. N. Gribov and B. Pontecorvo, Phys. Lett. B **28**, 493 (1969).
- [9] L. Wolfenstein, Phys. Rev. D **17**, 2369 (1978); S. P. Mikheyev and A. Yu. Smirnov, Sov. J. Nucl. Phys. **42**, 913 (1985).
- [10] N. Arkani-Hamed, S. Dimopoulos, and G. R. Dvali, Phys. Lett. B **429**, 263 (1998); I. Antoniadis, N. Arkani-Hamed, S. Dimopoulos, and G. R. Dvali, Phys. Lett. B **436**, 257 (1998); N. Arkani-Hamed, S. Dimopoulos, and G. R. Dvali, Phys. Rev. D **59**, 086004 (1999).
- [11] P. Minkowski, Phys. Lett. B **67**, 421 (1977); M. Gell-Mann, P. Ramond, and R. Slansky, in *Supergravity*, p. 315, edited by F. Nieuwenhuizen and D. Freedman, North Holland, Amsterdam, 1979; T. Yanagida, *Proceedings of the Workshop on Unified Theory and Baryon Number in the Universe*, edited by O. Sawada and A. Sugamoto, KEK, Tsukuba, Japan, 1979; R. N. Mohapatra and G. Senjanović, Phys. Rev. Lett. **44**, 912 (1980).
- [12] K. R. Dienes, E. Dudas, and T. Gherghetta, Nucl. Phys. B **557**, 25 (1999).
- [13] N. Arkani-Hamed, S. Dimopoulos, G. R. Dvali, and J. March-Russell, Phys. Rev. D **65**, 024032 (2001).
- [14] G. R. Dvali and A. Y. Smirnov, Nucl. Phys. B **563**, 63 (1999).
- [15] R. Barbieri, P. Creminelli, and A. Strumia, Nucl. Phys. B **585**, 28 (2000).
- [16] R. N. Mohapatra, S. Nandi, and A. Pérez-Lorenzana, Phys. Lett. B **466**, 115 (1999); R. N. Mohapatra and A. Pérez-Lorenzana, Nucl. Phys. B **576**, 466 (2000); R. N. Mohapatra and A. Pérez-Lorenzana, Nucl. Phys. B **593**, 451 (2001).
- [17] H. Davoudiasl, P. Langacker, and M. Perelstein, Phys. Rev. D **65**, 105015 (2002).
- [18] P. A. N. Machado, H. Nunokawa, and R. Zukanovich Funchal, Phys. Rev. D **84**, 013003 (2011).
- [19] F. P. An *et al.* (Daya Bay Collaboration), Phys. Rev. D **90**, 071101(R) (2014).
- [20] J. H. Choi *et al.* (RENO Collaboration), arXiv:1511.05849 [hep-ex].
- [21] Y. Abe *et al.* (Double Chooz Collaboration), J. High Energy Phys. **1410**, 086 (2014) [J. High Energy Phys. **1502**, 074 (2015)].
- [22] F. Capozzi *et al.*, Phys. Rev. D **89**, 093018 (2014).
- [23] J. Huang, Ph.D. Thesis, University of Texas at Austin (2015), FERMILAB-THESIS-2015-06.
- [24] P. Huber, M. Lindner, and W. Winter, Comput. Phys. Commun. **167**, 195 (2005); P. Huber *et al.*, Comput. Phys. Commun. **177**, 432 (2007).
- [25] A. Esmaili, O. L. G. Peres, and Z. Tabrizi, J. Cosmol. Astropart. Phys. **12**, 002 (2014).
- [26] K. A. Olive *et al.* (Particle Data Group), Chin. Phys. C **38**, 090001 (2014).
- [27] P. Adamson *et al.* (MINOS Collaboration), Nucl. Instrum. Meth. A **806**, 279 (2016).
- [28] D. G. Michael *et al.* (MINOS Collaboration), Nucl. Instrum. Meth. A **596**, 190 (2008).
- [29] T. M. Cover and P. E. Hart, IEEE Trans. Inf. Theory **13**, 21 (1967).
- [30] J. L. Bentley, Commun. ACM **18**, 509 (1975).
- [31] J. S. Marshall, Ph.D. Thesis, University of Cambridge (2008), FERMILAB-THESIS-2008-20.
- [32] P. Adamson *et al.* (MINOS Collaboration), Phys. Rev. Lett. **106**, 181801 (2011).
- [33] C. J. Backhouse, Ph.D. Thesis, University of Oxford (2012), FERMILAB-THESIS-2011-17.
- [34] G. Tinti, Ph.D. Thesis, University of Oxford (2010), FERMILAB-THESIS-2010-44.
- [35] P. Adamson *et al.* (MINOS Collaboration), Phys. Rev. Lett. **107**, 011802 (2011).
- [36] R. Ospanov, Ph.D. Thesis, University of Texas at Austin (2008), FERMILAB-THESIS-2008-04.
- [37] J. S. Y. M. Ratchford, Ph.D. Thesis, University of Texas at Austin (2012), FERMILAB-THESIS-2012-40.
- [38] M. Kordosky, Ph.D. Thesis, University of Texas at Austin (2004), FERMILAB-THESIS-2004-34.
- [39] J. S. Mitchell, Ph.D. Thesis, University of Cambridge (2011), FERMILAB-THESIS-2011-54.
- [40] M. Bonesini, A. Marchionni, F. Pietropaolo, and T. Tabarelli de Fatis, Eur. Phys. J. C **20**, 13 (2001).
- [41] C. Alt, *et al.* (NA49 Collaboration), Eur. Phys. J. C **49**, 897 (2007).
- [42] P. Adamson *et al.* (MINOS Collaboration), Phys. Rev. Lett. **108**, 191801 (2012).

- [43] S. V. Cao, Ph.D. Thesis, University of Texas at Austin (2014), FERMILAB-THESIS-2014-07. (1998).
- [44] G. J. Feldman and R. D. Cousins, Phys. Rev. D **57**, 3873